Synthesis and Structure of the Cluster Ion Pair $\{Ru_3(CO)_9[\mu\text{-}P(NPr^i_2)_2]_3\}\{Ru_6(CO)_{15}(\mu_6\text{-}C)[\mu\text{-}P(NPr^i_2)_2]\}$. A Theoretical Overview of $M_3(\mu\text{-}PR_2)_3$ Frameworks

Weibin Wang,[†] Paul J. Low,[†] Arthur J. Carty,*[,†] Enrico Sappa,[‡] Giuliana Gervasio,*[,§] Carlo Mealli,*[,∥] Andrea Ienco,[∥] and Enrique Perez-Carreño[∥,⊥]

Steacie Institute for Molecular Sciences, National Research Council of Canada, 100 Sussex Drive, Ottawa, Ontario, K1A 0R6, Canada, Dipartimento di Chimica Inorganica, Chimica Fisica e Chimica dei Materiali, Università degli Studi di Torino, Via P. Giuria, 7, 10125 Torino, Italy, Università del Piemonte Orientale "Amedeo Avogadro", C.so Borsalino 54, 15100 Alessandria, Italy, and Istituto per lo Studio della Stereochimica ed Energetica dei Composti di Coordinazione, CNR, Via Nardi 39, 50132 Firenze, Italy

Received February 18, 1999

The compound $\{Ru_3(CO)_9[\mu\text{-}P(NPr^i_2)_2]_3\}\{Ru_6(CO)_{15}(\mu_6\text{-}C)[\mu\text{-}P(NPr^i_2)_2]\}$ (**1**), obtained via the addition of $PCl(NPr^i_2)_2$ to $K_2[Ru_4(CO)_{13}]$, crystallizes in the monoclinic space group $P2_1/c$ with $a = 15.537(8)$ Å, $b = 36.151(16)$ Å, $c = 19.407(5)$ Å, $\beta = 91.14(2)°$, $Z = 4$, and $R = 0.069$ for 8006 observed reflections. The unit cell is unusual in that it contains both a typical octahedral Ru_6 cluster anion (**1a**), featuring an encapsulated carbide, and a symmetrical phosphido bridge, in addition to a 50-electron trinuclear cluster cation $\{Ru_3(CO)_9[\mu\text{-}P(NPr^i_2)_2]_3\}^+$ (**1c**). The latter, with approximate D_{3h} symmetry, exhibits long Ru−Ru distances (≥3.15 Å). Among the family of clusters with $M_3(\mu\text{-}PR_2)_3$ cores and different numbers of both electrons (TEC) and terminal ligands ($L_xL_yL_z$), **1c** is unique in that it is a 333 stereotype with 50 valence electrons. MO calculations permit us to predict the existence of redox congeners of **1c** clusters and related 48e Re_3 clusters. This work also presents a summary of the relationships between the electronic and the geometric structures for all known $M_3L_xL_yL_z(\mu\text{-}PR_2)_3$ species. The basic stereochemical features are influenced by the total-electron count and, hence, by the degree of M−M bonding, as well as the remarkable flexibility of the phosphido bridging ligands. The $\mu\text{-}PR_2$ ligands need not necessarily lie in the M_3 plane, and a wide range of M−P−M angles (as small as 72° or as large as 133°) have been observed.

Introduction

Metal-cluster compounds give rise to a remarkably diverse range of structures that continue to challenge synthetic and theoretical chemists alike. Over the years, many elegant theoretical approaches have been developed to provide order to this vast structural array, ranging from simple semiempirical models, such as the effective atomic number (EAN) and Wade−Mingos rules, to extended Hückel molecular orbital (EHMO) theory and ab initio methods.[1]

In any organometallic cluster, the M_n core will be supported by a variety of terminal and bridging ligands. A detailed description of the MO architecture for these complexes requires careful consideration of not only the number of cluster valence electrons that are available for bonding but also the stereochemistry and geometry of the supporting ligands. In this context, clusters that contain phosphido ligands (PR_2) bridging M···M vectors are particularly interesting because of the great structural flexibility of this ligand. This structural diversity is illustrated for the common framework $M_3(\mu\text{-}PR_2)_3$ (I) in Table 1.[2] In addition to the phosphido bridges, these complexes feature a variety of terminal ligands at each metal center (L_x, L_y, L_z) and electron counts ranging from 42 to 54 valence electrons.

In this paper, we report the synthesis and characterization of an unusual, discrete polymetallic salt $\{Ru_3(CO)_9[\mu\text{-}P(NPr^i_2)_2]_3\}\{Ru_6(CO)_{15}(\mu_6\text{-}C)[\mu\text{-}P(NPr^i_2)_2]\}$ **1**. The cluster cation **1c** is the first example of a 50-electron cluster cation with overall D_{3h} symmetry and three terminal ligands on each metal atom. We have taken the opportunity to compare the structural and bonding features not only between **1c** and the electron-precise Re_3 analogues **4** and **5** but also across the entire range of $M_3L_xL_yL_z(\mu\text{-}PR_2)_3$ clusters reported in Table 1. An analysis of the effects of the different electron populations and framework geometries on cluster bonding, based on qualitative MO theory, is presented with the arguments highlighted through the usage of the MO graphics package CACAO.[28]

* Author to whom correspondence should be addressed
† Steacie Institute for Molecular Sciences.
‡ Università degli Studi di Torino.
§ Università del Piemonte Orientale.
∥ Istituto per lo Studio della Stereochimica ed Energetica dei Composti di Coordinazione, CNR.
¶ Present address: Departamento de Química Física y Analítica, Universidad de Oviedo, Spain.

(1) Mingos, D. M. P.; Wales, D. J. *Introduction to Cluster Chemistry*; Prentice-Hall: Englewood Cliffs, NJ, 1990; p 93.
(2) *Cambridge Structural Database System*, Version 5.15, Cambridge Crystallographic Data Centre: Cambridge, CB2 1EZ, U.K.
(3) Deppisch, B.; Schafer, H.; Binder, D.; Leske, W. *Z. Anorg. Allg. Chem.* **1984**, *519*, 53.
(4) Haupt, H.-J.; Balsaa, P.; Florke, U. *Inorg. Chem.* **1988**, *27*, 280.
(5) Haupt, H.-J.; Florke, U.; Schneider, H. *Acta Crystallogr., Sect. C* **1991**, *47*, 2531.
(6) Dunn, P.; Jeffery, J. C.; Sherwood, P. *J. Organomet. Chem.* **1986**, *311*, C55.
(7) Asseid, F.; Browning, J.; Dixon, K. R.; Meanwell, N. J. *Organometallics* **1994**, *13*, 760.

10.1021/ic990195f CCC: $19.00
Published on Web 02/18/2000

Table 1. Trinuclear Species with $M_3(\mu\text{-}PR_2)_3$ Cores[a]

complex	type	metals/T.E.C.	phosph subst	M_1-M_2 (Å)	M_2-M_3 (Å)	M_3-M_1 (Å)	τ_{1-2} (deg)	τ_{2-3}(deg)	τ_{3-1} (deg)	ref
2	4,4,4	Mn_3/54	H	4.30	4.30	4.36	104	104	cpl	3
3	3,3,3[b]	Ni_3/54	H	3.81	3.81	3.81	138	138	138	4
1c	3,3,3	Ru_3/50	NPr^i_2	3.17	3.17	3.15	cpl	cpl	cpl	
4	3,3,3	Re_3/48	phen	2.91	2.91	2.92	cpl	cpl	cpl	4
5	3,3,3	Re_3/48	cychex	2.91	2.91	2.92	cpl	cpl	cpl	5
6	4,2,2[c]	WCo_2/48	Eth	3.00	2.71	2.68	170	cpl	102	6
7	3,3,2[d]	Ir_3/50	phen	3.03	3.22	3.29	cpl	cpl	170	7
8	3,2,2	Ir_3/50	phen	3.18	3.33	3.20	cpl	169	cpl	8
9	3,2,2	Rh_3/50	phen	3.12	3.25	3.13	174	164	cpl	9
10	3,2,2	Rh_3/50	phen	3.08	3.22	3.12	cpl	167	cpl	9
11	3,2,2[e,f]	Ir_3/48	phen	2.86	2.71	2.96	174	107	cpl	7
12	2,2,2	Co_3/48	cychex	2.68	2.57	2.58	cpl	119	119	10
13	2,2,2	Co_3/48	phen	2.66	2.57	2.57	168	114	120	11
14	2,2,2	Co_3/48	meth	2.63	2.51	2.57	156	110	137	12
15	2,2,2[g]	Ir_3/48	phen	3.00	2.71	2.97	cpl	108	157	13
16	2,2,2	Pt_3/48	spec[h]	4.05	4.08	4.22	95	123	148	14
17	2,2,2[i]	Zn_3/54	phen	4.14	4.26	4.16	127	173	117	15
18	2,2,1[f]	Ir_3/46	phen	2.74	2.80	2.80	104	cpl	cpl	8
19	2,2,1[f]	Rh_3/46	phen	2.76	2.80	2.80	103	172	172	8
20	2,2,1	Rh_3/46	but[t]	2.81	2.79	2.73	116	cpl	151	16
21	2,2,1	Rh_3/46	phen	2.70	2.81	2.79	97	171	171	9, 17
22	2,1,1[i,l]	Zn_3/50	cychex	4.15	4.05	4.16	152	144	152	18
23	1,1,1[i]	Zn_3/48	$SiMe_3$	4.10	4.26	4.14	135	151	cpl	19
24	1,1,1[i]	Zn_3/48	$SiMe_3$	3.86	4.28	4.07	110	156	173	19
25	1,1,1	Ag_3/48	phen	4.15	4.16	4.17	cpl	119	127	20
26	1,1,1[i]	Cd_3/48	but[t]	4.43	4.54	4.55	150	143	cpl	21
27	1,1,1	Rh_3/42	but[t]	2.67	2.67	2.64	cpl	cpl	163	22
28	1,1,1[j]	Pd_3/44	phen	3.00	2.95	2.95	cpl	cpl	cpl	23
29	1,1,1	Pt_3/42	spec[k]	2.75	2.73	2.74	cpl	173	cpl	24
30	1,1,1[m]	Pt_3/44	phen	3.07	2.96	2.96	cpl	159	159	25, 26
31	1,1,1[m]	Pt_3/44	phen	3.59	2.76	2.76	cpl	174	174	26
32	1,1,1[g,n]	Pt_3/44	but[t]	3.60	2.71	2.72	cpl	cpl	cpl	27

[a] Extracted from the Cambridge Structural Database (April 1998).[2] No additional atomic bridge between metals is allowed. Unless specified, the terminal ligands are two-electron donors, such as CO, RCN, or phosphine. M−M distances are reported in the order for L_xM-L_yM, L_yM-L_zM, and L_zM-L_xM (*x*, *y*, and *z* are the respective numbers of terminal ligands in the column labeled "type"). For each intermetallic vector, the dihedral angle (τ_{x-y}) is calculated between the planes M_3 and M_2P. The two planes are indicated as coplanar (cpl) if $175° < |\tau_{x-y}| < 180°$. [b] All of the L_3M fragments are CpNi. [c] The fragment L_4M is Cp(CO)W. [d] The unit is cationic. The second fragment L_3M contains a methyl anion. [e] The fragment L_3M is (CO)(OH)(I)Ir. [f] One bidendate ligand, $Ph_2PCH_2PPh_2$ (dppm), provides one terminal P donor to each L_2M fragment. [g] The geometric parameters are given as averages between two independent molecules. [h] A formally two-electron reduced P_4S_3 cage uses the P atoms of the broken P−P as terminal and bridging ligands, respectively. [i] One alkyl terminal ligand at each metal atom. [j] The L_2M fragment is completed by a tetrahydrofuran ligand. [k] One terminal chloride ligand at M_3. [l] R and R′ phosphido substituents are *tert*-butylimino- and *tert*-butyltrimethylsilyl-amino groups, respectively [m] One terminal phenyl ligand at M_3. [n] One terminal hydride ligand at M_3.

Experimental Section

General Procedure. Synthetic manipulations were performed in a nitrogen-atmosphere glovebox. The solvents were dried and distilled under nitrogen prior to use. The reagents were commercially supplied and used without further purification. Infrared spectra were recorded on a Nicolet 520 FTIR spectrometer. NMR spectra were recorded on Bruker AC-200 ($^{31}P\{^1H\}$ at 81.02 MHz) or Bruker AC-250 (^1H at 250.0 MHz) instruments. Mass spectroscopy was performed on a JEOL JMS-AX505H mass spectrometer, using FAB ionization techniques.

Preparation of $\{Ru_3(CO)_9[\mu\text{-}P(NPr^i_2)_2]_3\}\{Ru_6(CO)_{15}(\mu_6\text{-}C)[\mu\text{-}P(NPr^i_2)_2]\}$ (1). A mixture of $Ru_3(CO)_{12}$ (562 mg, 0.879 mmol), benzophenone, and potassium (molar ratio 1/1.5/1.5) was treated with THF (20 mL) over a 10 min period. The solution was stirred for 24 h, yielding a deep red solution. Subsequently, $PCl(NPr^i_2)_2$ (353 mg, 1.32

(8) Berry, D. E.; Browning, J.; Dehghan, K.; Dixon, K. R.; Meanwell, N. J.; Phillips, A. J. *Inorg. Chem.* **1991**, *30*, 396.
(9) Haines, R. J.; Steen, N. D. C. T.; English, R. B. *J. Chem. Soc., Dalton Trans.* **1984**, 515.
(10) Albright, T. A.; Kang, S.-K.; Arif, A. M.; Bard, A. J.; Jones, R. A.; Leland, J. K.; Schwab, S. T. *Inorg. Chem.* **1988**, *27*, 1246.
(11) Markiewicz, M. K.; Fraser, M. E.; Ungar, R. K.; Fortier, S.; Baird, M. C. *Acta Crystallogr., Sect. C* **1985**, *41*, 336.
(12) Keller, E.; Vahrenkamp, H. *Chem. Ber.* **1979**, *112*, 2347.
(13) Browning, J.; Dixon, K. R.; Meanwell, N. J. *Inorg. Chim. Acta* **1993**, *213*, 171.
(14) Di Vaira, M.; Peruzzini, M.; Stoppioni, P. *J. Chem. Soc., Dalton Trans.* **1985**, 291.
(15) Davidson, M. G.; Edwards, A. J.; Paver, M. A.; Raithby, P. R.; Russell, C. A.; Steiner, A.; Verhorevoort, K. L.; Wright, D. S. *J. Chem. Soc., Chem. Commun.* **1995**, 1989.
(16) Arif, A. M.; Heaton, D. E.; Jones, R. A.; Kidd, K. B.; Wright, T. C.; Whittlesey, B. R.; Atwood, J. L.; Hunter, W. E.; Zhang, H. *Inorg. Chem.* **1987**, *26*, 4065.
(17) Haines, R. J.; Steen, N. D. C. T.; English, R. B. *J. Organomet. Chem.* **1981**, *209*, C34.
(18) Edwards, A. J.; Paver, M. A.; Raithby, P. R.; Russell, C. A.; Wright, D. S. *Organometallics* **1993**, *12*, 4687.
(19) Rademacher, B.; Schwarz, W.; Westerhausen, M. *Z. Anorg. Allg. Chem.* **1995**, *621*, 287.
(20) Eisenmann, J.; Fenske, D.; Simon, F. *Z. Anorg. Allg. Chem.* **1995**, *621*, 1681.
(21) Benac, B. L.; Cowley, A. H.; Jones, R. A.; Nunn, C. M.; Wright, T. C. *J. Am. Chem. Soc.* **1989**, *111*, 4986.
(22) Atwood, J. L.; Hunter, W. E.; Jones, R. A.; Wright, T. C. *Inorg. Chem.* **1983**, *22*, 993.
(23) Arif, A. M.; Heaton, D. E.; Jones, R. A.; Nunn, C. M. *Inorg. Chem.* **1987**, *26*, 4228.
(24) Scherer, O. J.; Konrad, R.; Guggolz, E.; Ziegler, M. L. *Chem. Ber.* **1985**, *118*, 1.
(25) Bender, R.; Braunstein, P.; Dedieu, A.; Ellis, P. D.; Huggins, B.; Harvey, P. D.; Sappa, E.; Tiripicchio, A. *Inorg. Chem.* **1996**, *35*, 1223.
(26) (a) Taylor, N. J.; Chieh, P. C.; Carty, A. J. *J. Chem. Soc., Chem. Commun.* **1975**, 448. (b) Bender, R.; Braunstein, P.; Tiripicchio, A.; Tiripicchio Camellini, M. *Angew. Chem., Int. Ed. Engl.* **1985**, *24*, 861.
(27) Leoni, P.; Manetti, S.; Pasquali, M.; Albinati, A. *Inorg. Chem.* **1996**, *35*, 6045.
(28) (a) Mealli, C.; Proserpio, D. M. *J. Chem. Educ.* **1990**, *67*, 399. (b) Mealli, C.; Ienco, A.; Proserpio, D. M. *Book of Abstracts of the XXXIII ICCC*, Florence, 1998, 510.

Table 2. Crystallographic Data for 1

emp. form.	$C_{73}N_8O_{24}P_4Ru_9 \cdot C_{3.5}$	fw	2248.35 g/mol
a (Å)	15.537(8)	space grp	$P2_1/c$
b (Å)	36.15(2)	T (K)	293
c (Å)	19.407(5)	λ (Å)	0.710 73
β°	91.140(1)	ρ_{calc} (g cm^{-3})	1.492
V (Å^3)	10 898(8)	μ (Mo, Kα) (cm$^{-1)}$	1.329
Z =	4	R (F_o)	0.0689[a,b]
		Rw_2 (F_o)	0.192[c]

[a] $F_o > 4\sigma(F_o)$. [b] $R = \sum||F_o| - |F_c||/\sum|F_o|$. [c] $wR_2 = [\sum[w(F_o^2 - F_c^2)^2]/\sum[w(F_o^2)^2]]^{1/2}$, w = $1/[\sigma 2(F_o)^2 + (0.0999P)^2 + 212.50P]$ where $P = (\max(F_o^2,0) + 2F_c^2)/3$.

mmol, 2 × 0.75 equiv to $Ru_3(CO)_{12}$) was added in dropwise fashion, and the reaction was allowed to proceed for an additional 3 h. After the solvent was removed, the residue was extracted into CH_2Cl_2 and absorbed onto dried silica gel. The stained silica gel was dried in vacuo. Column chromatography (silica gel, 70−230 mesh, oven dried, 150 °C, 48 h), with CH_2Cl_2 as the eluant, following an initial elution with hexane and CH_2Cl_2/hexane (v/v = 1/1), led to the isolation of the product **1**. Air-stable, dark red crystals of **1** (10 mg, <2%) suitable for X-ray analysis were obtained from CH_2Cl_2/toluene at −10 °C. IR (CH_2Cl_2) ν (cm^{-1}): (CO) 2078 (w), 2051 (m), 2004 (s), 1992 (vs), 1935 (w), 1802 (br,w). ^{1}H NMR ($CDCl_3$): δ 4.29 (m, 3(C*H*)), 3.90 (m, 1(C*H*)), 1.49 (d, J_{HH} = 6.9 Hz, 6(CH_3)), 1.35 (d, J_{HH} = 7.0 Hz, 2(CH_3)). ^{31}P{^{1}H} NMR ($CDCl_3$): δ 131.8 (s, 3P), 346.0 (s, 1P). MS: (FAB$^+$, *m*/*z*) 1250.3; (FAB$^-$, *m*/*z*) 1270.5.

X-ray Analysis. Intensity data from a crystal of **1** were collected on a Siemens P4 diffractometer with the use of graphite-monochromated Mo Kα radiation (λ = 0.710 73 Å). A total of 15 452 reflections were collected at room temperature with a variable scan rate; for each reflection, the background was measured (stationary crystal-stationary counter) for 35% of the total scan time, at the beginning and end of the scan. Two intensity standards, monitored every 50 reflections during the data collection, showed a slight decay. No absorption correction was applied.

The positions of the metal atoms were determined by direct methods. Subsequent electron density difference maps revealed the remaining nonhydrogen atoms. No hydrogen atoms were introduced because of the thermal motion of the atoms bearing them; all of the nonhydrogen atoms were given anisotropic thermal parameters. A molecule of toluene appeared in the last Fourier-difference maps, and carbon atoms were introduced into the refinement as rigid groups with an occupancy factor of 0.5. All of the computations were carried out using SHELXTL PLUS 93 (PC version) software.[29] Crystallographic data and intensity-collection and -refinement parameters are summarized in Table 2, whereas the selected bond lengths and angles are shown in Table 3.

EHMO Calculations. In the MO calculations of the extended Hückel type,[30] a weighted Wolfsberg−Helmholz formula,[31] as implemented within the CACAO package, was employed.[28] Default parameters for the Slater Type Orbitals of the various metal atoms were employed. The molecular geometries were derived from the experimental structures that were retrieved from the CSD files; these geometries best adapted to the EHMO calculation through the Molecular Editor available in CACAO98,[28b] which, among other features, allows the automatic adaptation of a molecule to the nearest symmetry-point group.

The details of the DFT calculations are given in the Supporting Information.

Results and Discussion

The reaction of $PCl(NPr^i_2)_2$ with $K_2[Ru_4(CO)_{13}]$[32] predominantly yields $Ru_4(CO)_{13}[P(NPr^i_2)_2)]_2$.[33] Following extensive chromatography and crystallization, a second, minor component (**1**) was successfully isolated. This compound forms the subject of the current report.

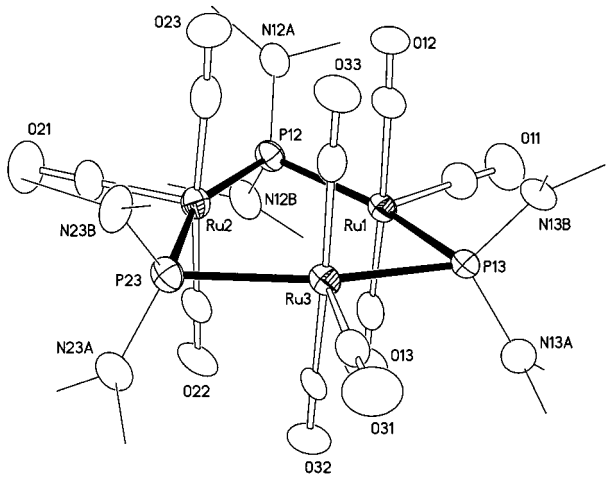

Figure 1. ORTEP diagram (30% probability) of the cation $\{Ru_3(CO)_9[\mu\text{-}P(NPr^i_2)_2]_3\}^+$ (**1c**).

Table 3. Selected Bond Lengths (Å) and Angles (deg) for 1

Bond Lengths (Å)			
Ru(1)−Ru(2)	3.171(3)	Ru(1)−Ru(3)	3.167(3)
Ru(2)−Ru(3)	3.150(3)	Ru(1)−P(12)	2.417(6)
Ru(1)−P(13)	2.408(6)	Ru(2)−P(12)	2.421(5)
Ru(2)−P(23)	2.419(5)	Ru(3)−P(13)	2.409(5)
Ru(3)−P(23)	2.395(5)		
Ru(4)−Ru(5)	2.982(3)	Ru(4)−Ru(7)	2.828(2)
Ru(4)−Ru(8)	2.909(2)	Ru(4)−Ru(9)	2.852(2)
Ru(5)−Ru(6)	2.939(3)	Ru(5)−Ru(8)	2.808(3)
Ru(5)−Ru(9)	2.936(2)	Ru(6)−Ru(7)	2.831(3)
Ru(6)−Ru(8)	2.944(3)	Ru(6)−Ru(9)	2.869(2)
Ru(7)−Ru(8)	2.946(2)	Ru(7)−Ru(9)	2.872(3)
Ru(5)−P(58)	2.321(6)	Ru(8)−P(58)	2.316(6)
Ru(4)−C(47)	2.03(3)	Ru(7)−C(47)	2.17(2)
Ru(6)−C(67)	1.92(3)	Ru(7)−C(67)	2.35(2)
Ru−C(0)av	2.05(2)		
Bond Angles (deg)			
P(13)−Ru(1)−P(12)	157.0(2)	Ru(1)−P(12)−Ru(2)	81.9(2)
P(23)−Ru(2)−P(12)	157.7(2)	Ru(1)−P(13)−Ru(3)	82.2(2)
P(23)−Ru(3)−P(13)	158.4(2)	Ru(3)−P(23)−Ru(2)	81.7(2)

The ^{1}H NMR spectrum of **1** showed two sets of signals for isopropyl groups with a ratio of ∼3:1, suggesting the existence of $P(N^iPr_2)_2$ ligands in two different chemical environments. The ^{31}P{^{1}H} NMR spectrum exhibited two singlets, at 131.8 and 346.0 ppm, with a ratio of 3:1, consistent with the ^{1}H NMR spectrum. The solution IR spectrum indicated the presence of both terminal and bridging carbonyl ligands. The FABMS of **1**, in the positive mode, contained an ion with *m*/*z* = 1250.3, whereas the negative FABMS also gave a group of isotopic peaks with the highest mass fragment at *m*/*z* 1270.5.

A single-crystal X-ray analysis of **1** revealed the presence of $\{Ru_3(CO)_9[\mu\text{-}P(NPr^i_2)_2]_3\}$ cation (**1c**) and $\{Ru_6(CO)_{15}(\mu_6\text{-}C)[\mu\text{-}P(NPr^i_2)_2]\}$ anion (**1a**) in the asymmetric unit cell (Figures 1 and 2). Complexes consisting of an ion pair of organometallic fragments are rare, especially when both of the fragments are metal clusters.[34]

The X-ray analysis showed that anion **1a** consists of an octahedral Ru_6 skeleton with an encapsulated μ_6-carbide ligand,

(29) Sheldrick, G. M. SHELXTL IRIS, Siemens Analytical X-ray Instruments Inc., Madison, WI, 1990.
(30) (a) Hoffmann, R.; Lipscomb, W. N. *J. Chem. Phys.* **1962**, *36*, 2872. (b) Hoffmann, R.; Lipscomb, W. N. *J. Chem. Phys.* **1962**, *37*, 3489.
(31) Ammeter, J. H.; Bürgi, H.-B.; Thibeault, J. C.; Hoffmann, R. *J. Am. Chem. Soc.* **1978**, *100*, 3686.
(32) Bhattacharyya, A. A.; Nagel, C. C.; Shore, S. G. *Organometallics.* **1983**, *2*, 1187.
(33) Corrigan, J. F.; Dinardo, M.; Doherty, S.; Hogarth, G.; Sun, Y.; Taylor, N. J.; Carty, A. J. *Organometallics* **1994**, *13*, 3572.

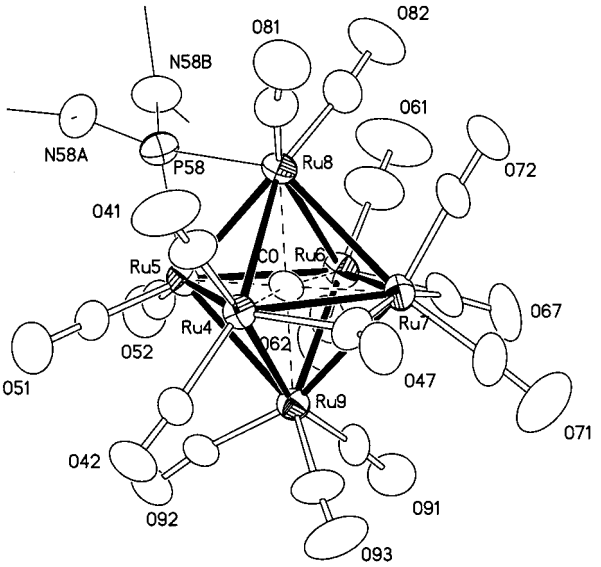

Figure 2. ORTEP diagram (30% probability) of the anion $\{Ru_6(CO)_{15}(\mu_6\text{-}C)[\mu\text{-}P(NPr^i_2)_2]\}^-$ (**1a**).

similar to other well-characterized $Ru_6(\mu_6\text{-}C)$ clusters.[35] The presence of two bridging carbonyl ligands is consistent with the solution IR data. With the exception of Ru(9), which bears three carbonyl ligands, the metal vertices of the cluster anion are coordinated by two terminal carbonyl ligands and one bridging carbonyl or phosphido ligand. The phosphido ligand symmetrically bridges Ru(5) and Ru(8).

The M−M bonds in the anion of **1** vary from 2.808 to 2.982 Å (Table 3), with the shortest being bridged by the phosphido ligand. The other bonds associated with Ru(5) or Ru(8) are relatively long. Although there are many examples of metal carbide clusters,[35−37] and the gross features of the solid-state structure of **1a** are quite similar to that of $[Ru_6(CO)_{16}(\mu_6\text{-}C)]^{2-}$[35d] and $[Fe_6(CO)_{16}(\mu_6\text{-}C)]^{2-}$,[36] **1a** is an unprecedented example of a phosphido-substituted carbide cluster.

The Ru_3 cation **1c** possesses a virtually planar Ru_3P_3 framework with a phosphido ligand that symmetrically bridges each edge of a Ru_3 triangle. The Ru−Ru separations are long (i.e., in the range 3.15−3.17 Å) but this fact alone does not completely exclude the existence of fractional M−M bonds. All six of the Ru−P bonds lie in the range of 2.395−2.421 Å (Table 3), and the P−Ru−P angles are large (av P−Ru−P = 157.7°). The overall symmetry is approximately D_{3h}, as long as the geometric arrangement of the phosphido-ligand substituents is ignored. The nitrogen atoms of the NPr^i_2 groups appear to be sp^2 hybridized. However, because all of the PNC_2 planes are orthogonal to the associated RuPRu planes, it seems unlikely that the stability of the planar Ru_3P_3 skeleton is attributable to conjugation between the nitrogen and phosphorus p_π orbitals.

The 50-electron cationic cluster **1c** is the only trinuclear Ru_3 cluster with the bare planar skeleton **I** (Table 1), although there are a few examples of $Ru_3(\mu\text{-}PR_2)_3$ clusters that feature additional bridging ligands and nonplanar frameworks.[38−42] For example, in addition to the 322 arrangement of terminal CO ligands, the 48-electron complex $[Ru_3(\mu\text{-}PPh_2)_3(\mu\text{-}H)(CO)_7]$[38] and the 50-electron species $[Ru_3(\mu\text{-}PPh_2)_3(\mu\text{-}Cl)(CO)_7]$[39] feature a bridging hydride or chloride ligand spanning the unique $(CO)_2Ru-Ru(CO)_2$ bond. In comparison to the structure of the electron-precise hydride cluster, the metal framework of the more electron-rich chloride-bridged cluster is significantly expanded. However, in both of these examples, the doubly bridged $(CO)_2Ru-Ru(CO)_2$ vector is considerably shorter than the other two (2.80 vs 3.01 (av) Å and 2.93 vs 3.17 (av) Å, for the hydride and chloride bridged species, respectively).

The 222 clusters $[Ru_3\{1,2\text{-}(\mu\text{-}PPh)_2C_6H_4\}_2(CO)_6]$[40] (48-electron) and $[Ru_3(\mu\text{-}PPh_2)_3(\mu_3\text{-}\eta^2\text{-}PPhpy)(CO)_6]$[42] (50-electron) both feature a total of four phosphido bridges and approximately equilateral Ru_3 cores. Again, greater metal−metal separations are observed in the case of the more electron-rich species (av Ru−Ru distances of 3.10 vs. 2.83 Å), and a theoretical analysis of the bonding in $[Ru_3\{1,2\text{-}(\mu\text{-}PPh)_2C_6H_4\}_2(CO)_6]$ has been presented.[40] The complicated 50-electron 322-species $(CO)_6Ru_3(\mu_3\text{-}H)[\mu_2\text{-}P(C_6H_5)_2]_3[\mu_3\text{-}P(C_6H_5)(C_6H_4)]$[41] features a capping hydride ligand in addition to its four phosphido bridges. In this case, the Ru−Ru separations vary between 3.03 and 3.21 Å.

On the basis of the complexes structurally characterized to date, it appears that the planar unsupported M_3P_3 framework **I** (M = Ru) is only stable in the case of 50-electron clusters. The addition of bridging ligands, the reduction of the total number of cluster-valence electrons, or both, is accompanied by the displacement of the phosphido groups out of the Ru_3 plane. However, planar M_3P_3 skeletons, **I**, are known for 48-electron clusters with M = Re. The geometries of the 48-electron $Re_3(CO)_9(\mu\text{-}PR_2)_3$ clusters **4** and **5** (Table 1) are closely related to

(34) (a) Bruce, M. I.; Rodgers, J. R.; Snow, M. R.; Wong, F. S. *J. Chem. Soc., Chem. Commun*. **1980**, 1285. (b) Bruce, M. I.; Rodgers, J. R.; Snow, M. R.; Wong, F. S. *J. Organomet. Chem.* **1982**, *240*, 299. (c) Gifuentes, M. P.; Humphrey, M. G.; Skelton, B. W.; White, A. H. *J. Organomet. Chem.* **1996**, *507*, 163. (d) Chan, S.; Lee, S.-M.; Lin, Z.; Wong, W.-T. *J. Organomet. Chem.* **1996**, *510*, 219. (e) Corrigan, J. F.; Sun, Y.; Carty, A. J. *New. J. Chem.* **1994**, *18*, 77 and references therein.

(35) (a) Johnson, B. F. G.; Johnston, R. D.; Lewis, J. *J. Chem. Soc., Chem. Commun*. **1967**, 1057. (b) Mason, R.; Robinson, W. R. *J. Chem. Soc., Chem. Commun*. **1968**, 468. (c) Sirigu, A.; Bianchi, M.; Benedetti, E. *J. Chem. Soc., Chem. Commun*. **1969**, 596. (d) Bradley, J. S.; Ansell, G. B.; Hill, E. W. *J. Organomet. Chem.* **1980**, *184*, C33.

(36) (a) Churchill, M. R.; Wormald, J. *J. Chem. Soc., Dalton Trans.* **1974**, 2410. (b) Churchill, M. R.; Wormald, J.; Knight, J.; Mays, M. J. *J. Am. Chem. Soc.* **1971**, *93*, 3073.

(37) (a) Albano, V. G.; Chini, P.; Martinengo, S.; McCaffrey, D. J. A.; Strumolo, D.; Heaton, B. T. *J. Am. Chem. Soc.* **1974**, *96*, 8106. (b) Beringhelli, T.; D'Alfonso, G.; Molinari, H.; Sironi, A. *J. Chem. Soc., Dalton Trans.* **1992**, 689 and references therein. (c) Simerly, S. W.; Wilson, S. R.; Shapley, J. R. *Inorg. Chem*., **1992**, *31*, 5146. (d) Gong, J.-H.; Tsay, C.-W.; Tu, W.-C.; Chi, Y.; Peng, S.-M.; Lee, G. H. *J. Cluster Sci*. **1995**, *6*, 289. (e) Adatia, T.; Curtis, H.; Johnson, B. F. G.; Lewis, J.; McPartlin, M.; Jill, M. *J. Chem. Soc., Dalton Trans.* **1994**, 1109. (f) Johnston, D. H.; Stern, C. L.; Shriver, D. F. *Inorg. Chim. Acta* **1993**, *213*, 83. (g) Johnson, B. F. G.; Lewis, J.; Raithby, P. R.; Saharan, V. P.; Wong, W. T. *J. Organomet. Chem.* **1992**, *434*, C10. (h) Chisholm, M. H.; Hammond, C. E.; Johnston, V. J.; Streib, W. E.; Huffman, J. C. *J. Am. Chem. Soc.* **1992**, *114*, 7055. (i) Shaposhnikova, A. D.; Drab, M. V.; Kamalov, G. L.; Pasynskii, A. A.; Eremenko, I. L.; Nefedov, S. E.; Struchkov, Y. T.; Yanovskii, A. I. *J. Organomet. Chem.* **1992**, *429*, 109. (j) Chihara, T.; Yamazaki, H. *J. Organomet. Chem.* **1992**, *428*, 169. (k) Davies, D. L.; Jeffery, J. C.; Miguel, D.; Sherwood, P.; Stone, F. G. A. *J. Organomet. Chem.* **1990**, *383*, 463. (l) Jeffery, J. C.; Parrott, M. J.; Stone, F. G. A. *J. Organomet. Chem.* **1990**, *382*, 225. (m) Drake, S. R.; Johnson, B. F. G.; Lewis, J.; Nelson, W. W. J. H.; Vargas, M. D.; Adatia, T.; Braga, D.; Henrick, K.; McPartlin, M.; Sironi, A. *J. Chem. Soc., Dalton Trans.* **1989**, 1455. (n) Albano, V. G.; Braga, D.; Grepioni, F.; Della Pergola R.; Garlaschelli, L.; Fumagalli, A. *J. Chem. Soc., Dalton Trans*. **1989**, 879.

(38) Bullock, L. M.; Field, J. S.; Haines, R. J.; Minshall, E.; Moore, M. H.; Mulla, F.; Smit, D. N.; Steer, L. M. *J. Organomet. Chem.* **1990**, *381*, 429.

(39) Cabeza, J. A.; Lahoz, F. J.; Martin, A. *Organometallics* **1992**, *11*, 2754.

(40) Soucek, M. D.; Clubb, C. C.; Kyba, E. P.; Price, D. S.; Scheuler, V. G.; Aldaz-Palacios, H. O.; Davis, R. E. *Organometallics* **1994**, *13*, 1120.

(41) Corrigan, J. F.; Doherty, S.; Taylor, N. J.; Carty, A. J.; Boroni, E.; Tiripicchio, A. *J. Organomet. Chem.* **1993**, *462*, C24.

(42) Lugan, N.; Fabre, P.-L.; de Montauzon, D.; Lavigne, G.; Bonnet, J.-J.; Saillard, J.-Y.; Halet, J.-F. *Inorg. Chem.* **1993**, *32*, 1363.

1c, featuring 333 ligand sets and planar $M_3(\mu\text{-}PR_3)_3$ cores, but significantly shorter M−M separations.

In the following section, we shall discuss the stability of **1c** and the related, hypothetical 48-electron cluster $[Ru_3(CO)_9(\mu\text{-}PH_2)_3]^{3+}$, in addition to providing an overview of the structural features and M−M bonding found in some prototypal compounds reported in Table 1.

Overview of the $M_3(\mu\text{-}PR_2)_3$ Frameworks in Terms of the Qualitative MO Picture. The phosphido bridges play an important role in stabilizing this array of cluster types. By opening or closing the M−P−M angles and freely dislocating, with respect to the M_3 plane, the flexible μ-PR_2 bridges may adopt the most appropriate geometry to minimize M−M repulsion or to favor the metal-orbital hybridization necessary for M−M bonding (vide infra). To arrive at a comprehensive view of the bonding in clusters of structural type **I** (Table 1), we have employed EHMO methods and have chosen to illustrate the electronic structures of the clusters $M_3L_xL_yL_z(\mu\text{-}PH_2)_3$ via the graphic capabilities of the CACAO package.

In the 54-electron species **2**, **3**, and **17** with terminal sets 444, 333, and 222, respectively, the terminal ligands and phosphido bridges satisfy the electronic requirements of the metal atoms. Direct M−M bonding is therefore excluded, and the phosphido bridges act as the only collating agents for the cluster. The drawings **II**−**IV**show that the metal centers have stable, local d^6-octahedral (**2**, **II**), d^8-five coordinated (**3**, **III**), or d^{10}-tetrahedral (**17**, **IV**) geometry, respectively. In general, to

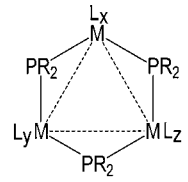

I

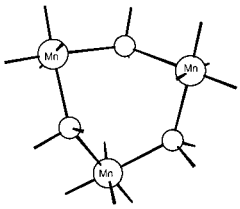

II

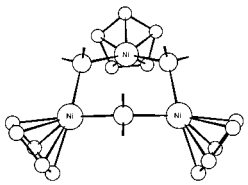

III

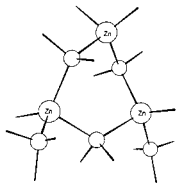

IV

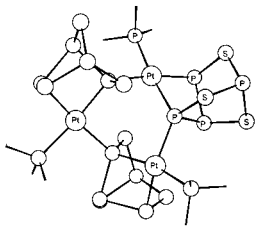

V

minimize the repulsive forces between the metal lone pairs, the framework **I** distorts from planarity and expands as much as possible (Table 1).

For cases in which the metal centers maintain vacant axial p_z orbitals and reach stable 16-electron configurations, local-planar coordination environments are observed at each metal, as is the case for **16**, **22**, and **23**−**26**. The 48-electron complex **16** (**V**) comprises three noninteracting square-planar Pt(II) ions, each coordinated by one terminal-phosphine ligand and by P atoms derived from two formally reduced P_4S_3 cages. Upon the oxidative addition of one P−P bond, each of the latter ligands contributes one terminal donor and one phosphido-like bridge to the cluster. The uniquely mixed typology observed in the 211 complex **22** results in an electron-precise 50-electron system. In this case, one tetrahedral (18-electron) and two planar (16-electron) Zn(II) centers coexist, with the whole assembly supported by phosphido bridging groups. In the case of the 48-electron species **23**−**26**, three-coordinated d^{10} Zn(II), Ag(I), or Cd(II) centers are simply collated by three phosphido-bridging ligands.

For the remaining systems of type **I**, a degree of overlap between the metal-based orbitals is evident. A planar-$M_3(\mu\text{-}PR_3)_3$ framework **I,** featuring an equilateral disposition of metal centers, requires the mutual mixing of radial and tangential orbitals. Although the overall MO picture **VI** refers to the 48-electron systems $M_3L_9(\mu\text{-}PH_2)_3$ (e.g., **4** or **5**), the pattern in the dashed box showing three filled bonding orbitals ($1e' + a_1'$) lying below three empty antibonding orbitals ($a_2' + 2e'$) is quite general. The single components represent one high-lying σ-hybrid and one lower d_π-orbital per metal. The bonding may also be described in terms of σ-aromaticity. This concept, introduced by Dewar for cyclopropane,[43] has previously been adapted to 42-electron triangular clusters such as the 111 Rh_3 and Pt_3 species **27** and **29**.[44] These 42-electron species are related to **4** and **5** in the same manner as mononuclear square planar 16-electron complexes are related to 18-electron octahedral examples.

The critical MO a_2' is formed by the same unhybridized d_π orbitals (t_{2g} origin for the square pyramidal fragments) that are responsible for the π-back-donation from the metal framework to the terminal CO ligands. The energy of a_2' is sensitive to the M−M separations, and a sizable destabilization of this orbital is reached with metals of the second or third transition row, for which the d_π orbitals, being more expanded, interact to a greater extent. Thus, in clusters of the heavier metals, this level may be vacant, giving rise to a HOMO−LUMO gap sufficiently large to ensure the system is thermodynamically stable. Significantly, first row metal analogues of the electron precise clusters **4**, **5**, **27**, and **29**, which on the basis of the orbital argument presented above would be predicted to feature smaller HOMO−LUMO gaps, have not yet been observed.

The 50-electron cluster **1c** features the same set of six basic MOs illustrated in **VI**. However, in the case of **1c**, the energy

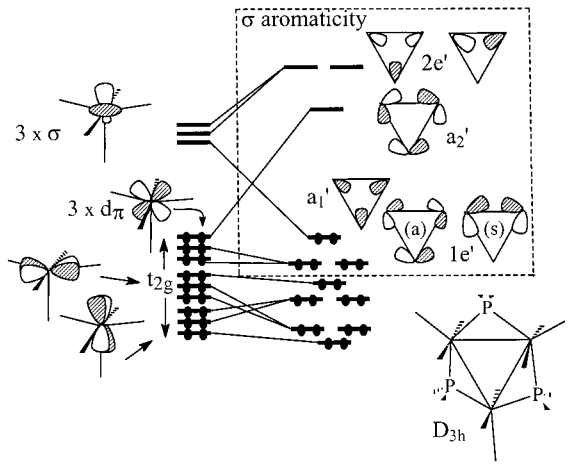

VI

of the a_2' orbital, which is now populated, is significantly

(43) Dewar, M. J. S. *J. Am. Chem. Soc.* **1984**, *106*, 669.
(44) Mealli, C. *J. Am. Chem. Soc.* **1985**, *107*, 2245.

reduced, approaching that of the other filled frontier orbitals. The possibility is then raised that population of this orbital will result not in cleavage of an M−M bond but rather in expansion of the M_3 core. In terms of a simple valence bond model, we would say that for **1c** and related 50-electron species the population of one antibonding orbital, in addition to the three bonding orbitals found in the 48-electron analogues, reduces the M−M bond order by one-third. Similar descriptions involving two M−M bonds delocalized over three metal centers have previously been applied to the comparable 44-electron systems **28** and **30**, which feature 111 ligand sets.[44]

The alternative structural motif, featuring two localized M−M bonds, has been observed (**31**, **32)**, and preliminary theoretical studies of this structural dichotomy underline the role played by the nature of the terminal ligands in determining the extent of M−M bonding within the framework **I**.[26] In the specific cases of **1c**, **4**, and **5**, the π-acceptor capabilities of the in-plane CO ligands could be an important factor for the preservation of the D_{3h} symmetry.

A descent from D_{3h} to C_{2v} symmetry would be accompanied by a reorientation of the two equivalent terminal ligands to positions almost trans to the M−M bonds, resulting in a mixing of some of the six critical MOs (**VI**). As shown in **VII**, the

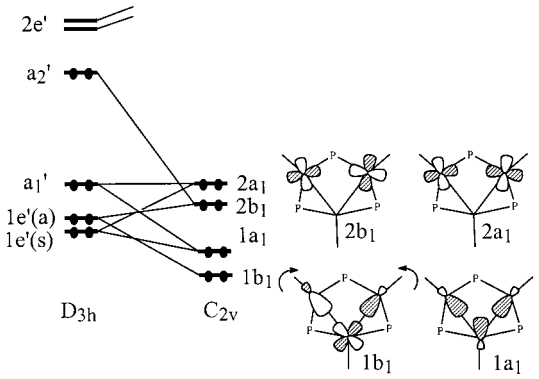

VII

former D_{3h} levels a_2' and $1e'$ (a) combine to give rise to a lone pair ($2b_1$, out-of-phase combination of d_π orbitals) and a bonding MO ($1b_1$). In the latter, the d_π lobes of the unique metal atom overlap with the two σ hybrids of the other metals. The other bonding MO $1a_1$ is similar to the a_1' orbital in **VI**, whereas $2a_1$ represents the in-phase lone pair combination of d_π orbitals at the symmetric metal atoms. It is worth mentioning that several attempts have been made to optimize, at the DFT level, the conformer of **1c** with a broken Ru−Ru linkage (see the Supporting Information). No matter how long the separation imposed on the latter, the C_{2v} model always converged to the expanded D_{3h} structure.

The Walsh diagram **VIII** illustrates the behavior of the frontier MOs of the 48-electron $M_3(CO)_9(\mu\text{-}PH_2)_3$ species along the ideal contraction/expansion pathway under D_{3h} symmetry (EHMO method). On the left-hand side of **VIII**, where the structure resembles that observed for **4** and **5**, the empty antibonding MO a_2' lies relatively high in energy, but it becomes more stable as the cluster is allowed to expand, as illustrated on the right-hand side of **VIII**.

For M−M separations near 3.5 Å, the system appears to be stable only if a_2' is populated. The 48- and 50-electron forms of $M_3(CO)_9(\mu\text{-}PR_2)_3$ therefore appear to be related by cluster expansion, rather than by M−M bond cleavage. The electrochemical reduction of the 48-electron system, to give a stable 50-electron species featuring an expanded M_3 framework, would

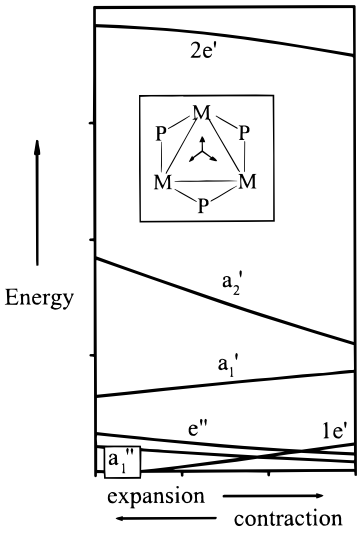

VIII

appear to be feasible. Also, it is likely that, in the absence of a_2'/a_1' interlevel crossing, the redox process may appear reversible in cyclovoltammetry. However, it must be pointed out that while these computations suggest thermodynamic stability of the reduced form of **4** and **5**, and imply the stability of the oxidized form of **1c**, the kinetic stability of these redox products cannot be assessed.

With respect to the electrochemical properties of these $M_3L_9(\mu\text{-}PR_2)_3$ systems, it is worth mentioning that the energy of the a_1' MO in the Ru_3 clusters is consistently higher than those found for the Re_3 analogues due to the larger contraction of Ru radial σ-hybrid orbitals. In fact, the Ru−Ru overlap populations are found to be consistently one-third that of the Re clusters. For the same reason, the HOMO−LUMO gap of the 48-electron Ru_3^{3+} species appears suspiciously small (~0.7 eV) as the cluster framework contracts. This small HOMO−LUMO gap may be taken as an indication of limited thermodynamic stability. Moreover, it cannot be excluded that, along the contraction/expansion pathway, a_2' can become lower than a_1'. Such a *forbidden level crossing* would also imply irreversibility between the redox isomers. On the other hand, it must be considered that the a_2' MO is related to the orbitals responsible for back-bonding into the CO ligands, so that, when this level is populated, the M−CO separations are shortened. In turn, these cause a more pronounced hybridization of the metal σ components in the MO a_1' and a constant stabilization below a_2'. Our DFT calculations fully confirm the latter point as the optimized structures of all the possible species $[M_3(CO)_9(\mu\text{-}PH_2)_3]^n$ (M = Ru, $n = 1+, 3+$; M = Re, $n = 0, 2-$) could be properly compared. Besides the expected expansion, the reduced 50e clusters show $M-C_{eq}$ bonds that are ~0.1 Å shorter than those found in the corresponding oxidized congeners. In addition, by using a scanning technique, the behavior of the frontier MOs along the contraction/expansion pathway (see **VIII**) was confirmed at the DFT level.

Following the completion of this work and during the submission of the manuscript, we learned of a similar theoretical study by Saillard and co-workers that describes the DFT-optimized geometry of the 50-electron model complex $[Ru_3(CO)_9(\mu\text{-}PH_2)_3]^+$ and the corresponding two-electron oxidized analogue $[Ru_3(CO)_9(\mu\text{-}PH_2)]^{3+}$.[45] These authors were unaware

(45) Garland, M. T.; Costuas, K.; Kahal, S.; Saillard, J.-Y. *New J. Chem.* **1999**, *23*, 509.

that we had prepared and structurally characterized the "missing" 50-electron cation $\{Ru_3(CO)_9[\mu\text{-}P(NPr^i_2)_2]_3\}^+$. In view of their (now published) results, we decided to limit our report on the DFT calculations and to mention only a few salient features. Thus, besides the already introduced reproduction of the Walsh-type diagram **VIII**, it is worth mentioning that our calculations are the first of this type available for known and predictable Re_3 redox derivatives. In general, although we were able to arrive at a satisfactory geometry for both Ru_3 and Re_3 48-electron species, excessively long M−M distances within the M_3P_3 frameworks of the 50-electron species were obtained (Ru−Ru 3.31 Å; Re−Re 3.52 Å). The divergence between the computational results obtained by the two groups for the M = Ru cluster model provides an insightful illustration of how the choice of the computational parameters is rather subtle and subjective in the DFT approach, especially for cases in which the potential energy curve is flat.

The MO picture established above for **1c**, **4**, and **5** may be used to rationalize the structure and bonding properties of the whole family of $M_3L_xL_yL_z(\mu\text{-}PR_2)_3$ complexes (**I**). The 50-electron systems **7**−**10** (Table 1) are closely related to **1c** and feature quasi-planar $M_3(\mu\text{-}PR_2)_3$ skeletons with M−M bonds involving rather elongated ML_2 fragment(s). Clusters **7** and **8**−**10** are 332 and 322 types, respectively, and are derived from the 333 structure by the removal of one or more axial ligands. In place of the "missing" ligand, each $ML_2(PR_2)_2$ metal center now carries an axial hybrid orbital that hosts a nonbonding electron pair (**IXa**). In addition, each metal center hosts in-plane x^2-y^2 and xy orbitals (**IXb**,**c**) that have the appropriate radial and tangential characteristics required for the reconstruction of the basic MO scheme shown in **VII**.

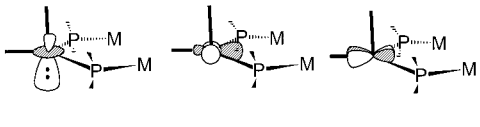

IX

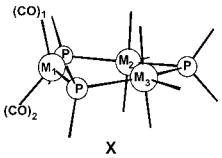

X

The relatively high energy z^2-based hybrid orbital(s), **IXa**, and indeed the system as a whole, is stabilized when the in-plane ligands are bent out of the M_3 plane ∼45° and lie along the nodal surface of this z^2-type orbital. Such a feature may be observed at the unique metal center of the cationic cluster $Ir_3(CH_3)(NCR)_3(CO)_4(\mu\text{-}PPh_2)_3]^+$ (**X**) and at the equivalent metal atoms in **8**−**10**.

For the sake of brevity, we do not present here a detailed analysis of the orbital mixings that occur during the evolution from the D_{3h} precursor to the ultimate C_s structure via a C_{2v} intermediate structure. However, molecular orbital overlap population (MOOP) diagrams[46] have been used to clearly identify the cause of the weaker M−M bonds observed in the clusters featuring ML_2 fragments. The frontier d_π hybrids of the $ML_2(PR_2)_2$ fragments are not seriously affected by a rotation of the ML_2 units, and the orbital lobes remain almost symmetrically oriented with respect to the M_3 triangle and are directed toward the center of the cluster. For a 332 cluster (i.e., **7**) the unique d_π hybrid orbital of the ML_2 fragment is directed toward nonhybridized d_π orbitals of the ML_3 fragments, resulting in an elongation of both the ML_3-ML_2 bonds with respect to the third. For a 322 model (**XI**), the filled hybrid orbitals associated with each ML_2 fragment repel each other strongly and elongate the associated ML_2-ML_2 bond. Therefore, the

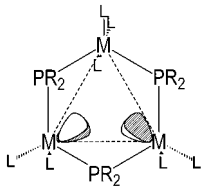

XI

geometry of these species is due to electronic repulsive forces between ML_2 metal-centered lone pairs rather than any innate reduction in the attractive forces between the metal centers.

In comparison with the 50-electron 322 clusters **8**−**10**, the unique, electron-precise (48-electron) 322 cluster **11** (**XII**) features a contracted M_3 core, a nonplanar M_3P_3 skeleton, and terminal hydroxo and iodo ligands. One of the MPM planes

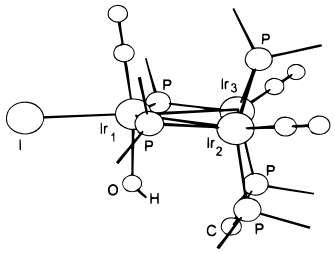

XII

has rotated such that the phosphido bridge sits above the M_3 plane, whereas the donor atoms of a bridging dppm ligand occupy the corresponding trans positions. A phosphido bridge and a carbonyl ligand, both of which are slightly out of the M_3 plane, complete the coordination environment of each metal. Apparently, the $Ir(CO)(\eta^1\text{-dppm})(\mu\text{-}PPh_2)$ pseudo-ML_4 fragments are not properly oriented to exploit their well-known σ and d_π hybrids in the basic network of radially and tangentially interacting orbitals (**VI**).

An EHMO analysis shows that the x^2-y^2 type orbitals, which are σ with respect to the pseudo-C_2 axis of the nonunique metal centers, use the orthogonal lobes for the basic tangential interactions. This is evident in the empty a_2'-type MO shown in **XIII**. This orbital lies relatively high in energy, close to the CO π^* levels. Population of a_2' to give a 50-electron system, and the resulting expansion of the M_3 core, is probably incompatible with the upright position of the phosphido bridge, and rearrangement to a planar structure similar to that observed for **8**−**10** would appear likely.

The mixed-metal cluster $CpMo(CO)_5Co_2(\mu\text{-}PEt_2)_3$, **6** (**XIV**), is another 48-electron cluster somewhat related to **11**. Although we did not attempt any specific MO analysis on this complicated molecule, some of its stereochemical features have already been described, such as the upright position of one phosphido bridge. Notice that, although the two Co atoms are coordinated by the same type and number of ligands, they adapt to different stereotypes. The atom Co1, bound on one side to the phosphido bridge uniquely out of the skeletal plane, adapts to the same

(46) MOOP = molecular orbital overlap population, that is, the contribution of a given MO to the overlap population of any chosen pair of atoms. This is a new feature available in the most recent version of the package CACAO.[28b]

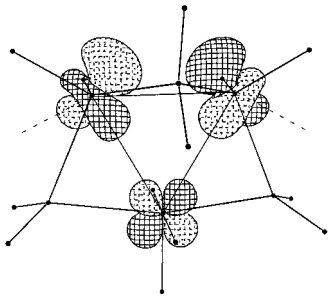

XIII

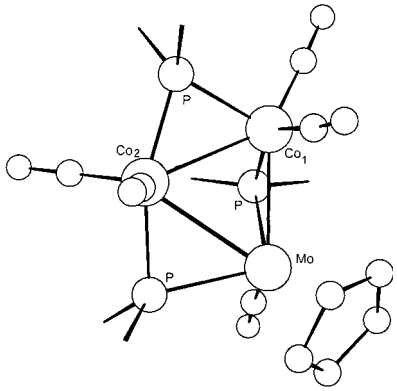

XIV

butterfly-type ML_4 already observed in **11**. Namely, one CO ligand is trans to the apical phosphido bridge. The coordination is completed in the plane by the second (quasi planar) CO and by the other phosphido bridge. Contrastingly, the atom Co2 is bound to two in-plane phosphido bridges; the unit ML_2 presents the same asymmetry with respect to the M_3 plane as that observed in the compounds **7**−**10**. Finally, the Cp(CO)Mo unit, assembled together with two phosphido bridges, is a pseudo-octahedron which can still use its t_{2g} orbitals for the intermetallic interactions.

The framework common to the 48-electron 222 structures **12**−**16** is depicted in **XV**. A detailed study of the bonding and

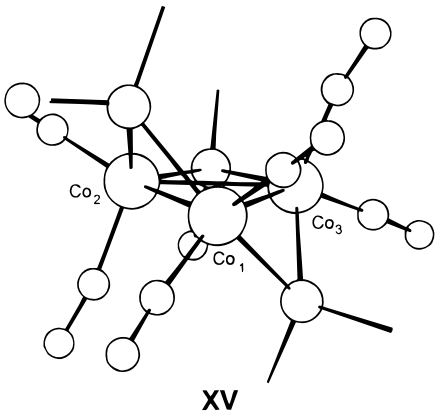

XV

fluxional behavior has been performed for **12**,[10] and according to these authors, the symmetric D_{3h} structure is always avoided. Essentially, three equivalent $L_4M\text{-}d^8$ butterfly fragments (i.e., with axial phosphido bridges in the plane M_3P_3 and equatorial CO ligands symmetrically displaced from the latter) are a source of electronic repulsion. The bonding in this case is an extension of the situation depicted in **XI**. The three filled d_π frontier orbitals are directed toward each other, causing significant M−M repulsion, while the tangential π-components necessary for the mutual in-plane interactions (**VI**) are derived from low-lying and nonhybridized t_{2g} levels. In no case does the MO a_2' rise to a sufficiently high energy to be unoccupied. Rather, a distortion of the **XI** geometry to **XV**, by displacing two μ-PR_2 ligands to opposite sides of the M_3 plane, occurs to yield the typical pattern of three bonding MOs lying below three orbitals that are antibonding with respect to the M−M bonds. Interestingly, a 50-electron dianion could be derived from **12** by chemical or electrochemical reduction.[10] According to the available computational data, the opening of one M−M bond would be preferred over the symmetric M_3 expansion.

The 221 46-electron systems **18**−**21** may be formally derived from the 48-electron **XII** structure by the removal of both axial ligands from the unique metal center. The unusual 46-electron count is consistent with loss of the two electrons from the z^2-type orbital of the 48-electron precursor. Steric interactions between the μ-PR_2 ligands would appear to be responsible for the additional distortions found in the structure of **21**.

Conclusions

This paper has presented the synthesis and characterization of a previously missing example of an $M_3L_9(\mu\text{-}PR_2)_3$ cluster with 50 valence electrons. This finding has prompted us to systematically analyze all of the known structures containing the $M_3(\mu\text{-}PR_2)_3$ framework. Basic qualitative perturbation theory concepts and EHMO calculations have been exploited in order to correlate the various structural arrangements with the number of terminal ligands and electron counts. For selected cases, DFT calculations were also made, to corroborate the results. In general, we point out conceptual continuity among the ∼30 compounds in which the $M_3(\mu\text{-}PR_2)_3$ core adapts to a variety of different electronic, bonding, and structural situations, and, for some of these species, it has also been possible to make predictions regarding the potential redox properties.

Acknowledgment. We thank the Natural Sciences and Engineering Research Council of Canada, the National Research Council of Canada and MURST (Italy) for financial support. E. P.-C. is grateful to the Spanish Ministerio de Educacion y Cultura for a Postdoctoral grant. P.J.L. held an NRC-NSERC Canadian Government Laboratories Visiting Fellowship. Financial support from EC Contract ERBIC15CT960746 is gratefully acknowledged. We also thank the "Area della Ricerca CNR di Firenze" (in particular, Dr. A. Tronconi and Mr. S. Cerreti) for the providing computing time and facilities.

Supporting Information Available: Details of the DFT optimized geometries of $[M_3(CO)_9(\mu\text{-}PH_2)_3]^n$ (M = Ru, n = 1+, 3+; M = Re, n = 0, 2−) and an X-ray crystallographic file in CIF format for the structure of $\{Ru_3(CO)_9[\mu\text{-}P(NPr^i_2)_2]_3\}\{Ru_6(CO)_{15}(\mu_6\text{-}C)[\mu\text{-}P(NPr^i_2)_2]\}$. This material is available free of charge via the Internet at http://pubs.acs.org.

IC990195F